AGU PUBLICATIONS

Geophysical Research Letters

Supporting Information for

Contrasting Trends and Drivers of Global Surface and Canopy Urban Heat Islands

Huilin Du[1], Wenfeng Zhan[1, 2*], James Voogt[3], Benjamin Bechtel[4], TC Chakraborty[5], Zihan Liu[1], Leiqiu Hu[6], Zhihua Wang[7], Jiufeng Li[1], Peng Fu[8], Weilin Liao[9], Ming Luo[9], Long Li[1], Shasha Wang[1], Fan Huang[1], and Shiqi Miao[1]

[1]Jiangsu Provincial Key Laboratory of Geographic Information Science and Technology, International Institute for Earth System Science, Nanjing University, Nanjing, Jiangsu 210023, China

[2]Jiangsu Center for Collaborative Innovation in Geographical Information Resource Development and Application, Nanjing, Jiangsu 210023, China

[3]Department of Geography, Western University, London, Ontario N6A 5C2, Canada

[4]Department of Geography, Ruhr-University Bochum, Bochum, Nordrhein-Westfalen 44801, Germany

[5]Atmospheric Sciences and Global Change Division, Pacific Northwest National Laboratory, Richland, Washington, 99352, USA

[6]Department of Atmospheric Science, University of Alabama in Huntsville, Huntsville, Alabama 35899, USA

[7]School of Sustainable Engineering and the Built Environment, Arizona State University, Tempe, Arizona 85287, USA

[8]Center for Environment, Energy, and Economy, Harrisburg, Pennsylvania 17101, USA

[9]Guangdong Key Laboratory for Urbanization and Geo-simulation, School of Geography and Planning, Sun Yat-sen University, Guangzhou, China

Contents of this file

Introduction

Supporting information includes two texts (Texts S1 to S2), twelve figures (Figures S1 to S12), and three tables (Tables S1 to S3).

- Text S1 shows the clarifications on the study area;
- Text S2 shows the uncertainties related to the impacts from accuracy of SAT estimates on the quantification of I_c trends.

- Figure S1 denotes the distribution of 5643 cities worldwide;
- Figure S2 shows the annual mean daytime I_s trends across 5643 cities worldwide quantified using different buffer zones to delineate the rural surfaces;
- Figure S3 gives the impacts from different sizes of buffer zones for delineating rural surfaces on the quantification of global mean daytime I_s trends;
- Figure S4 shows the trends of ΔDTR_{LST} and ΔDTR_{SAT};
- Figure S5 gives the annual mean LST and SAT trends across global cities as well as the associated global mean trends;
- Figure S6 shows the mean I_s and I_c trends for cities across various continents during the day and night;
- Figure S7 shows the mean ISP trends and EVI trends over urban and rural surfaces across different continents;
- Figure S8 gives the logarithmic relationships between daytime and nighttime I_s and I_c trends and urban population across global cities;
- Figure S9 shows the relative importance of various controls to global I_s and I_c trends in different seasons;
- Figure S10 gives the partial correlation coefficients (*r*) between the I_s and I_c trends and each driver across global cities;
- Figure S11 shows the statistical relationships between daytime I_s trends and $K_{\Delta EVI}$ as well as those between nighttime I_s trends and $K_{\Delta WSA}$ across global cities;
- Figure S12 shows the global mean daytime and nighttime I_c trends quantified based on spatially continuous SAT estimates and *in-situ* SAT measurements.

- Table 1 shows the details of the data used in this study;
- Table 2 shows the global warming trends based on LST and SAT over both urban and rural surfaces across global 5643 cities;
- Table 3 shows the abbreviations and symbols used in this study.

Text S1: Clarifications on the study area

The chosen 5643 cities are distributed in various climate zones (Figure S1), including equatorial (427 cities), arid (878 cities), temperate (2610 cities), snow (1718 cities), and polar climates (10 cities) according to the Köppen–Geiger classification scheme (Kottek et al., 2006). These cities are also distributed in six continents, including Asia (1822 cities), Europe (1381 cities), Africa (395 cities), North America (1593 cities), South America (340 cities), and Oceania (112 cities). In terms of city size, these cities can also be divided into four groups according to the quartile of urban population averaged from 2003 to 2020, labeled as POP-1, POP-2, POP-3, and POP-4 cities.

Text S2: *Uncertainties related to the impacts from accuracy of SAT estimates on the quantification of I_c trends*

This study employed the spatially continuous SAT estimates to examine the global I_c trends (Zhang et al., 2022). Although this product possesses much higher accuracy compared to other global SAT products, it may still introduce potential uncertainties into the quantification of global I_c trend. We have therefore further discussed these potential impacts on the I_c trend according to the Bessel formula. We have also performed cross-validations to demonstrate the robustness of the methods and results by comparing the global I_c trends calculated based on spatially continuous SAT products and *in-situ* SAT measurements.

(1) *Possible uncertainties related to the impacts from accuracy of SAT data according to Bessel formula*

The estimation accuracies of this SAT product are 1.20 °C to 2.44 °C for daily T_{max} and 1.69 °C to 2.39 °C for daily T_{min} on a per-pixel scale (Zhang et al., 2022). Nevertheless, these should not introduce large biases in the main results of the current study due to the following reasons. First, we have excluded the anomalies of SAT time series for each pixel, and then aggregated these daily SATs into monthly composites to reduce the impacts from data anomalies as well as to obtain climatologically representative SATs. Using these monthly SATs, we have further estimated the I_s and I_c trends for each city by first averaging the LSTs and SATs for all available urban and rural pixels and then subtracting the rural temperatures from the urban one. These temporal and spatial averaging procedures would generally suppress the impacts from SAT estimation accuracy on the quantification of I_c trend for an individual city according to the Bessel formula ($\frac{\delta}{\sqrt{n-1}}$, n represents the number of samples and δ denotes the SAT estimation error at the per-pixel scale; Pugachev, 2014; Ye et al., 2016). More importantly, the current study focuses mainly on the disparities between I_s and I_c trends on a global scale or across various climate zones that involve thousands or hundreds of cities. Therefore, the uncertainties arising from SAT estimation error to the quantification of I_c trend for an individual city would be further reduced once a large number of samples are averaged.

(2) Cross-validations of the robustness of this study with in-situ SAT measurements

In-situ SAT measurements from weather stations often possess relatively high data accuracy (about 0.1 K) and they offer an opportunity to perform cross-validations to demonstrate the robustness of the associated results. Using *in-situ* SAT measurements from more than 40,000 stations obtained from Berkey Earth and the China Meteorological Data Service Centre (Cao et al., 2016; Rohde et al., 2013), we further quantified the site-based global I_c trends in 461 cities worldwide and compared these trends with those quantified based on the spatially continuous SAT estimates to verify the reliability of our results (Figure S12). These 461 cities were selected based on the following criteria. First, we have initially identified all stations as 'urban' or 'rural' according to whether they are situated over urban or rural surfaces and whether the impervious surface percentage in the 200-m buffer around the station is greater or less than 20% in each year throughout the study period (Du et al., 2021). Second, we further screened the stations according to the data quality of their long-term SAT measurements. Specifically, we excluded the SAT outliers with the '3σ rule' for each station, and screened the stations with data missing rate (< 50%) in every single year throughout the study period. To ensure the representativeness of global cities, we slightly loosened the criteria (at least five years of data for both 2003 – 2010 and 2011 – 2020 and at least five months of data per year) for the less developed or developing regions owing to their extreme scarcity of weather stations. We finally obtained 660 urban and 953 rural stations that covering 461 cities worldwide and then quantified the I_c trends of these cities. The results revealed that the global mean I_c trends quantified based on *in-situ* SAT measurements are 0.04 K/decade for both daytime and nighttime (Figure S12), which are very close to those quantified based on the spatially continuous SAT estimates (i.e., 0.03 K/decade for both daytime and nighttime). These two distinct data sources show similar magnitudes of global UHI trends, strongly indicating the reliability of the main results of the current study.

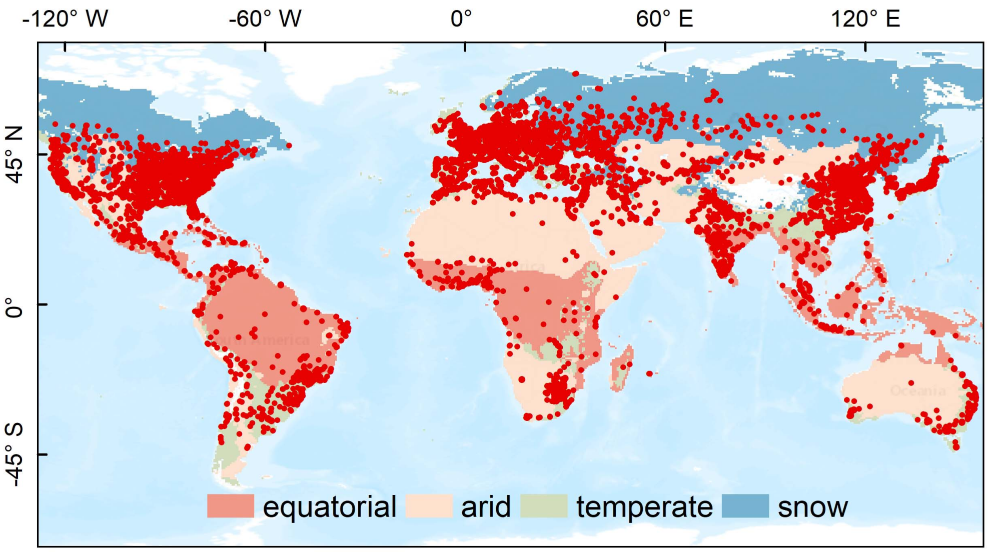

Figure S1. Distribution of 5643 cities worldwide.

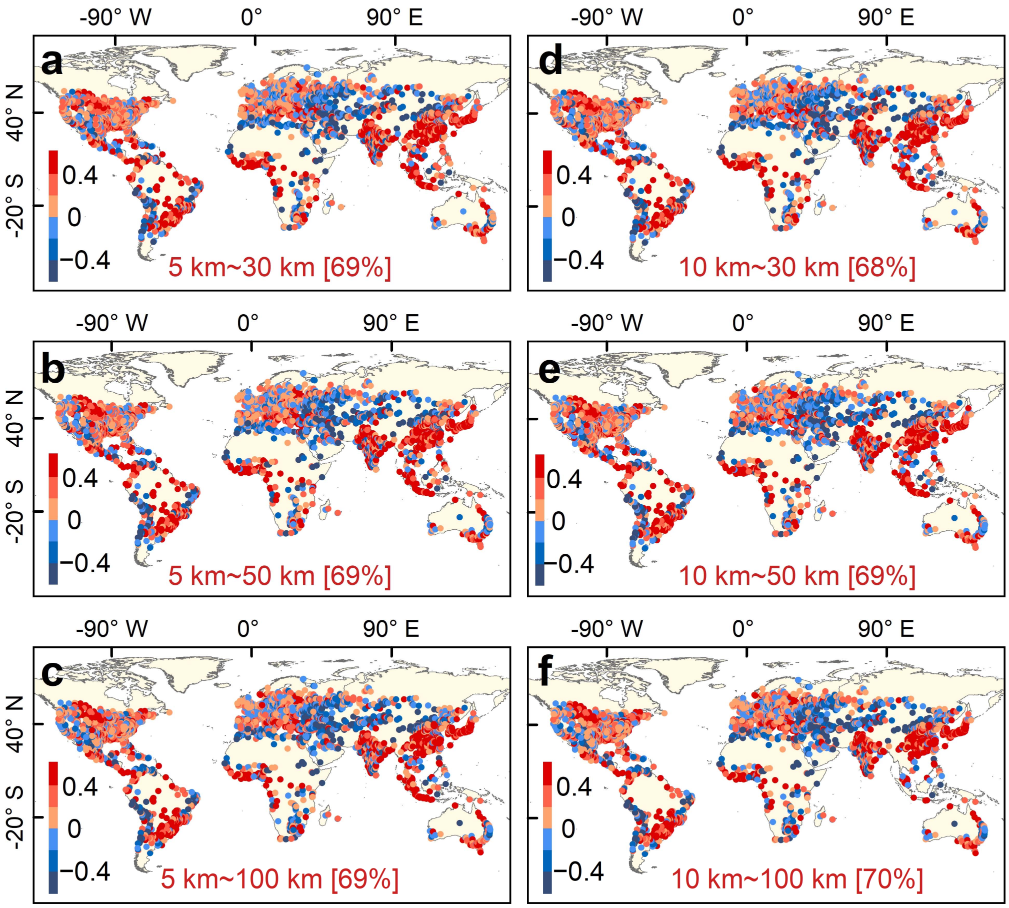

Figure S2. The annual mean daytime I_s trends across 5643 cities worldwide quantified using different buffer zones to delineate the rural surfaces.

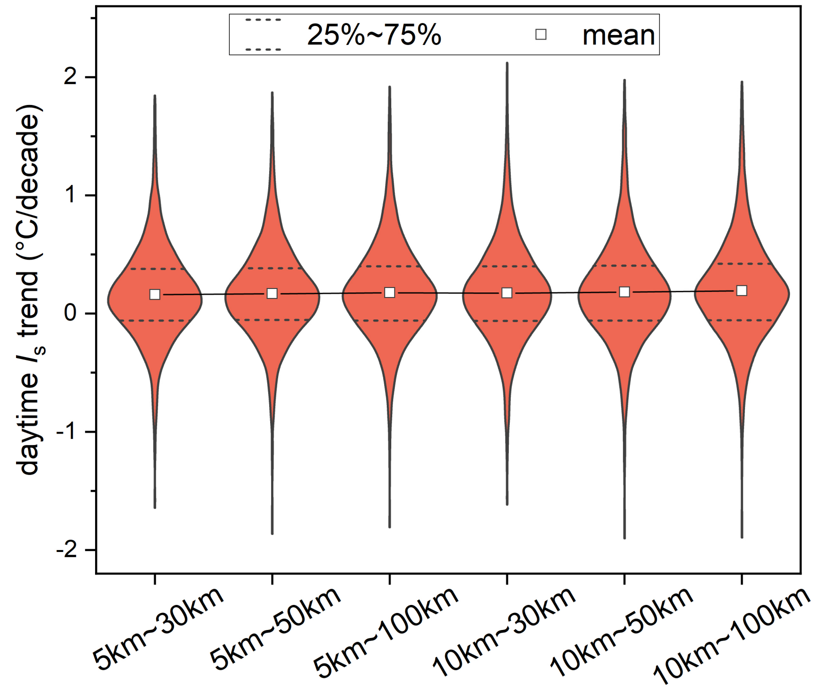

Figure S3. Impacts from different sizes of buffer zones for delineating rural surfaces on the quantification of global mean daytime I_s trends.

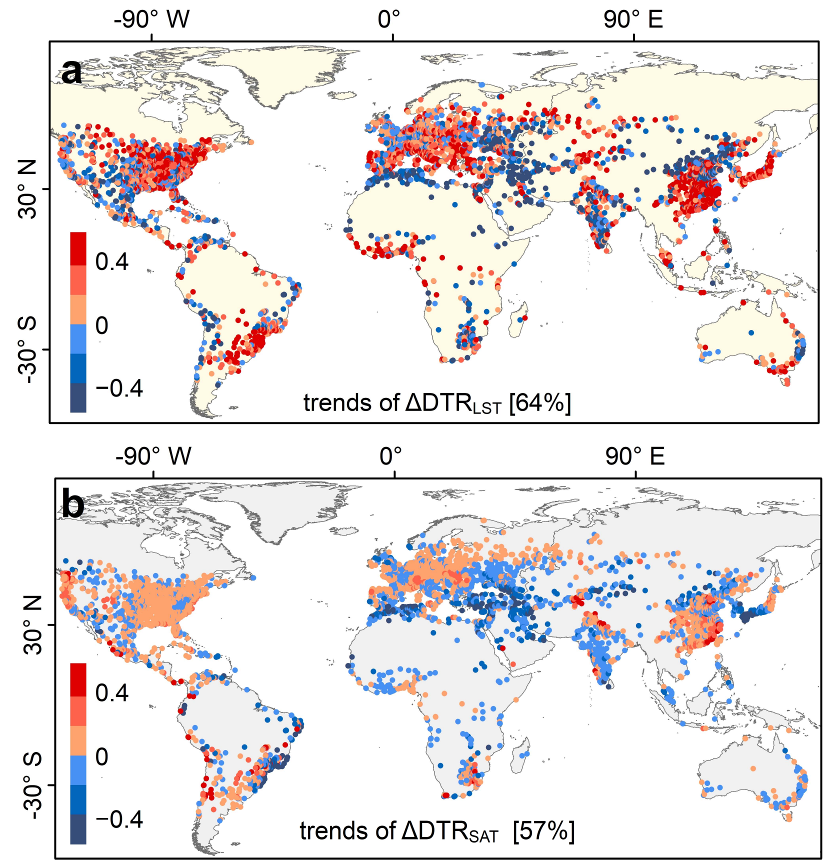

Figure S4. Trends of ΔDTR_{LST} (the LST-based diurnal temperature range variations induced by urbanization; a) and ΔDTR_{SAT} (the same as ΔDTR_{LST}, but for SAT; b) | The percentages in brackets indicate the proportion of cities with positive trends.

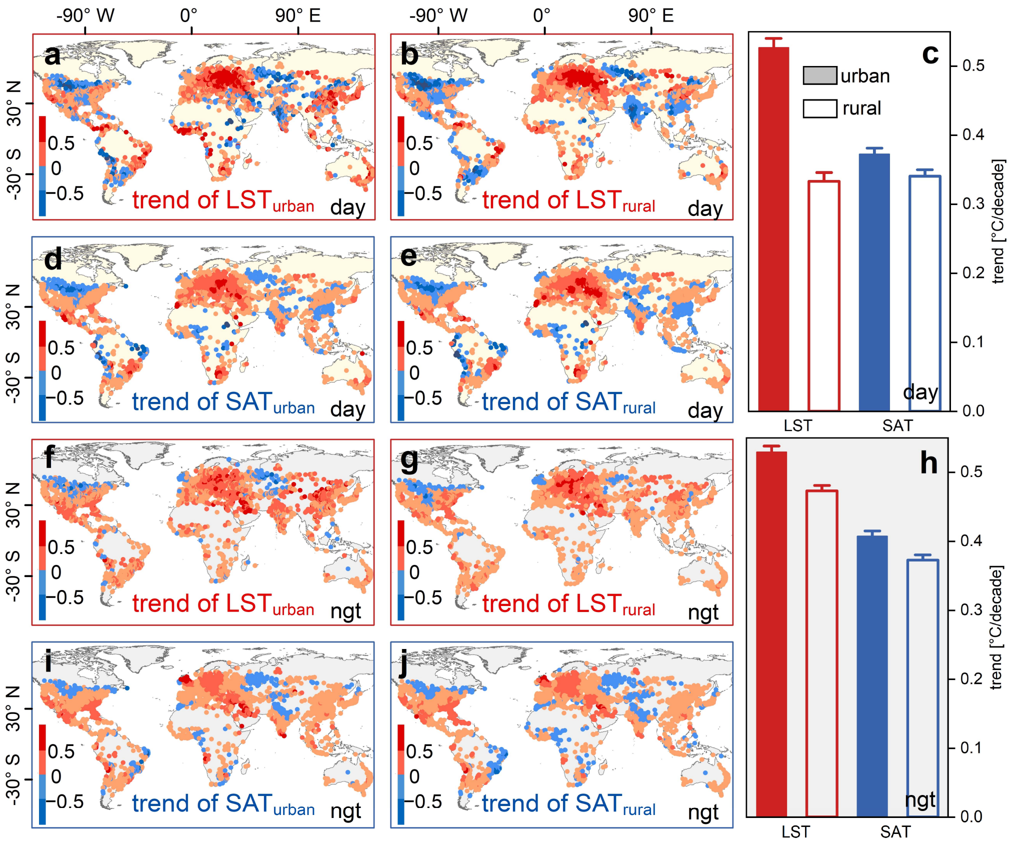

Figure S5. Annual mean LST and SAT trends across global cities as well as the associated global mean trends | The urban and rural LST trends and SAT trends city by city during the day (a, b, d, and e) and night (f, g, i, and j), and the global mean LST and SAT trends for the day (c) and night (h). The error bars in (c) and (h) denote the 90% confidence interval.

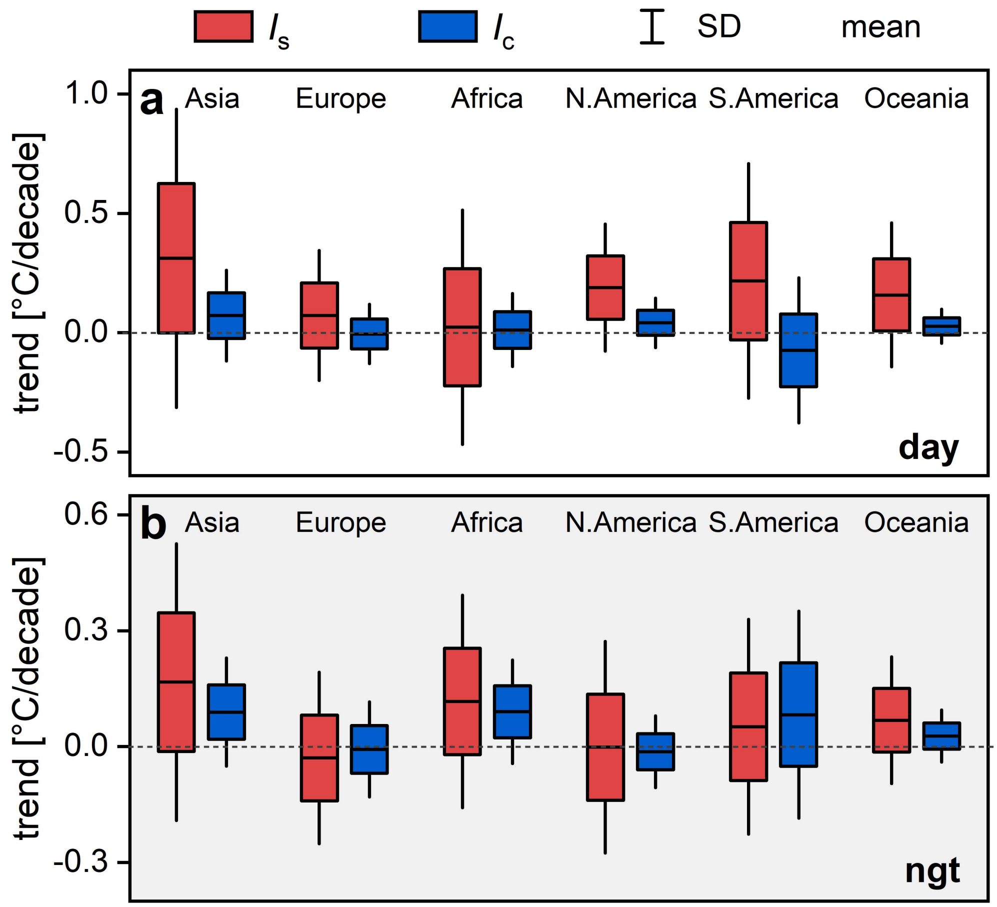

Figure S6. The mean I_s and I_c trends for cities across various continents during the day (a) and night (b).

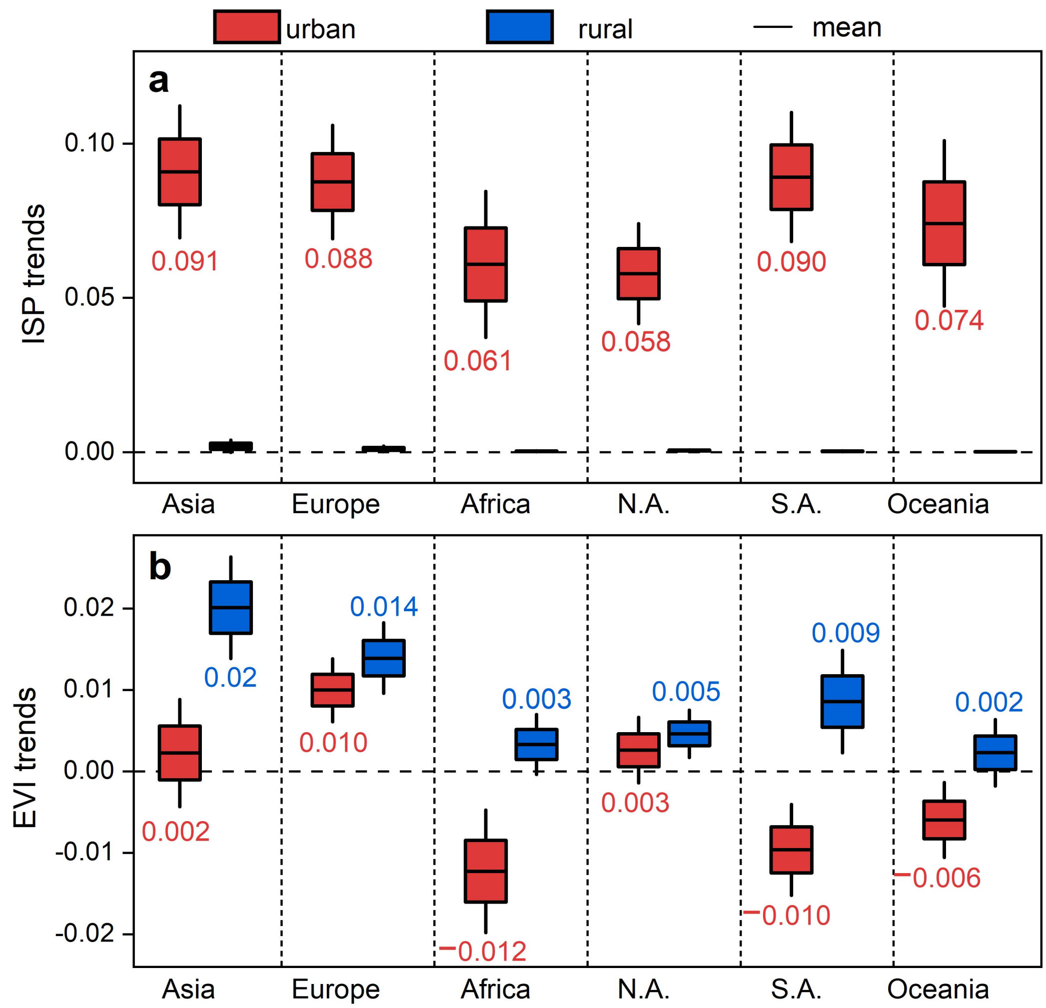

Figure S7. The mean ISP trends (a) and EVI trends (b) over urban (red) and rural (blue) surfaces across different continents, with the values signifying the magnitudes of associated ISP or EVI trends.

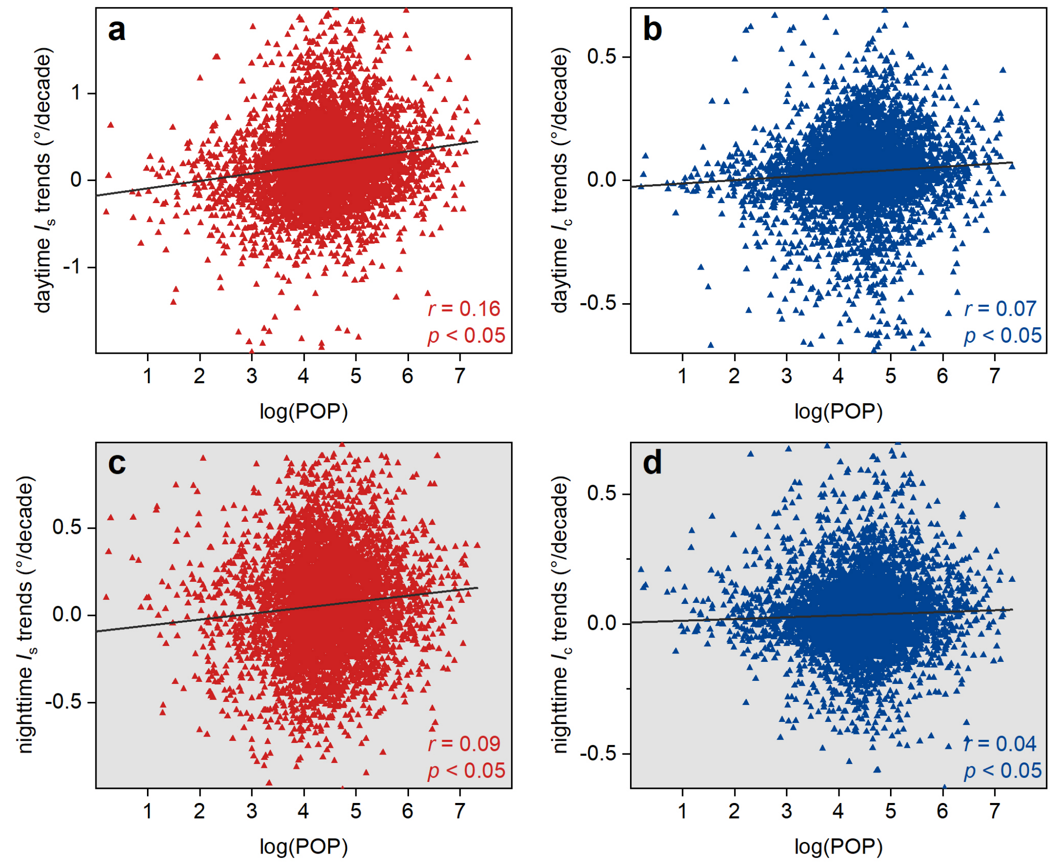

Figure S8. Logarithmic relationships between daytime and nighttime I_s and I_c trends and urban population across global cities.

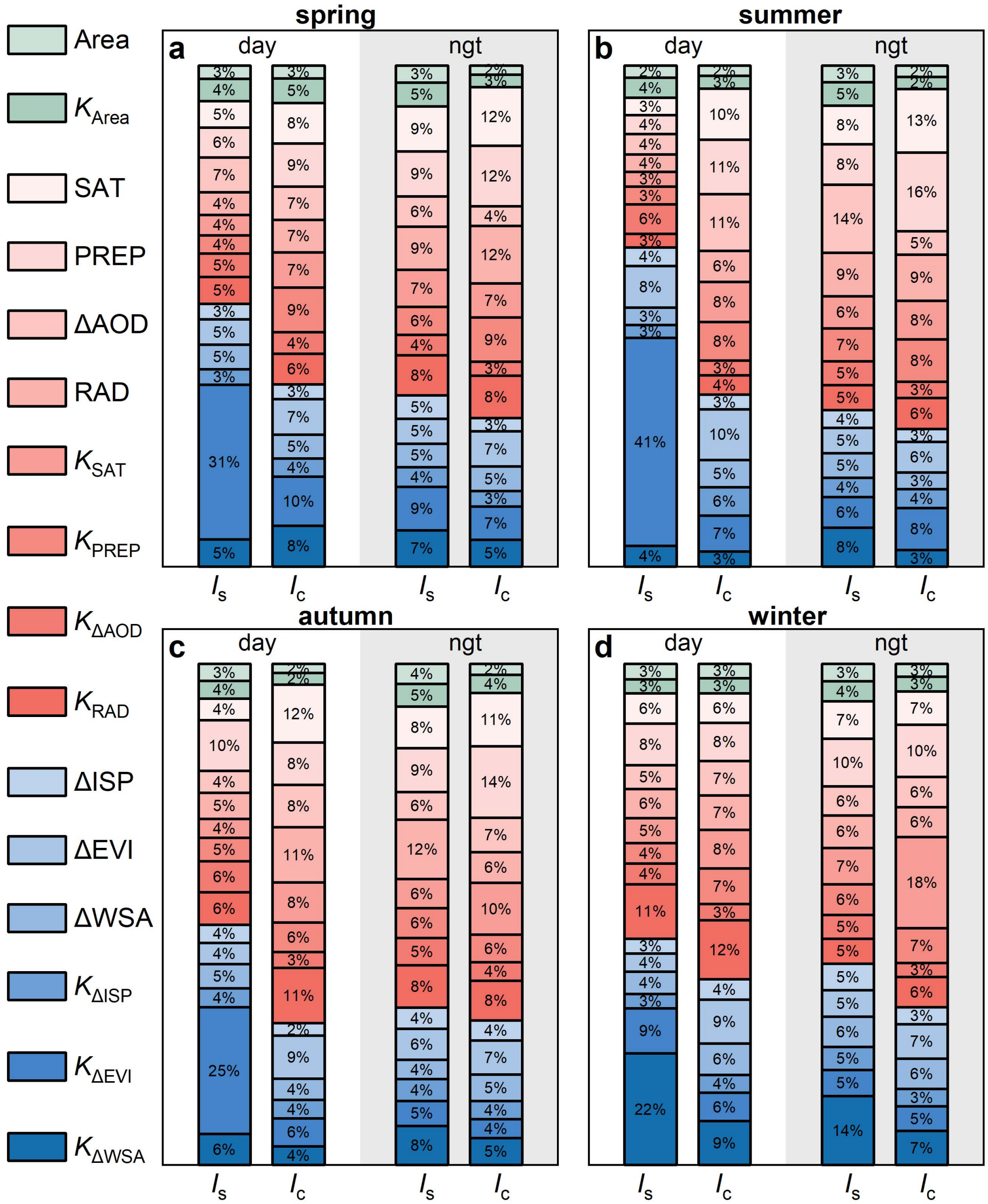

Figure S9. Relative importance of various controls to global I_s and I_c trends in different seasons | Panels (a), (b), (c), and (d) denote the results for spring, summer, autumn, and winter, respectively. Area and K_{Area} belong to the overall urban metric (OUM) category; SAT, PREP, ΔAOD, RAD, K_{SAT}, K_{PREP}, $K_{ΔAOD}$, and K_{RAD} belong to the background climate (BGC) category; and ΔISP, ΔEVI, ΔWSA, $K_{ΔISP}$, $K_{ΔEVI}$, and $K_{ΔWSA}$ belong to the surface property (SFP) category. The representations of these variables are given in the Material and methods of this manuscript.

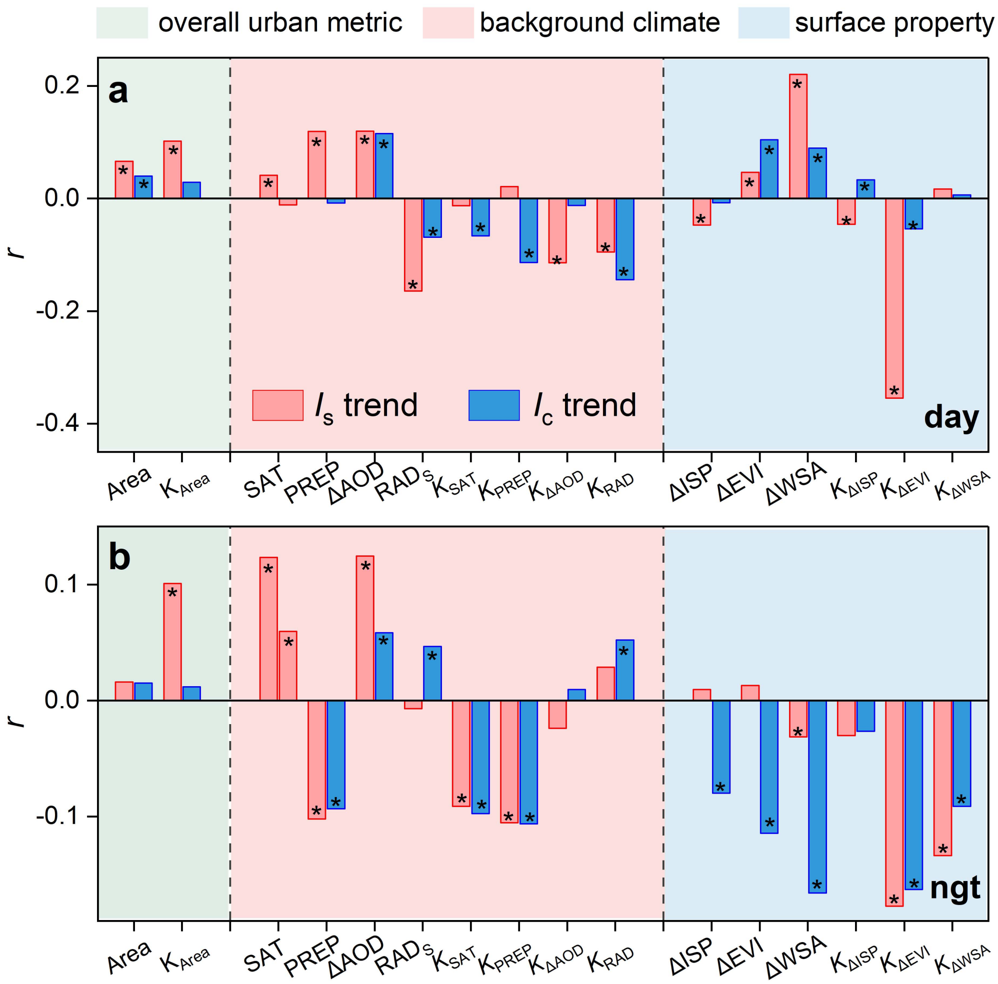

Figure S10. Partial correlation coefficients (r) between the I_s and I_c trends and each driver across global cities | (a) is for the day while (b) is for the night. The asterisk (*) indicates statistical significance at the 0.05 level. Area and K_{Area} belong to the overall urban metric (OUM) category; SAT, PREP, ΔAOD, RAD_s, K_{SAT}, K_{PREP}, $K_{ΔAOD}$, and K_{RADs} belong to the background climate (BGC) category; and ΔISP, ΔEVI, ΔWSA, $K_{ΔISP}$, $K_{ΔEVI}$, and $K_{ΔWSA}$ belong to the surface property (SFP) category. The representations of these variables are given in the Material and methods of this manuscript.

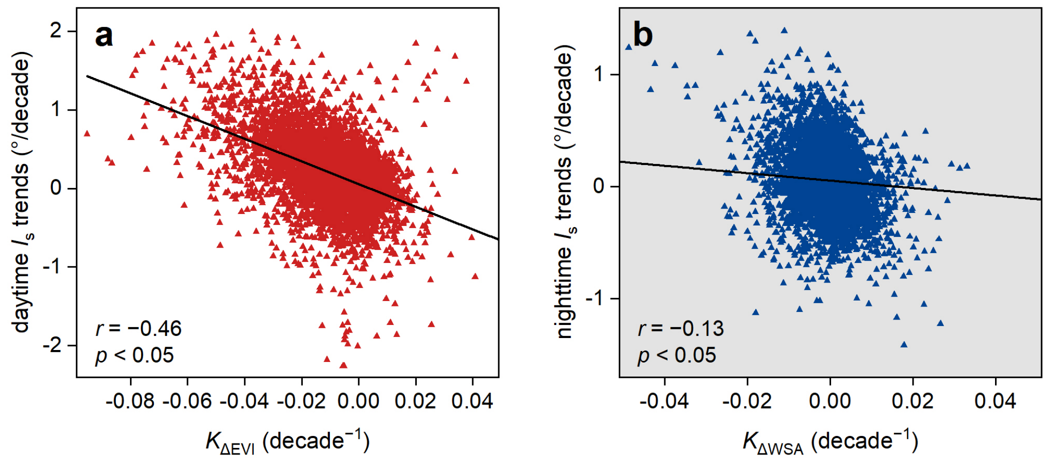

Figure S11. Statistical relationships between daytime I_s trends and $K_{\Delta EVI}$ (i.e., trend in ΔEVI; a) as well as those between nighttime I_s trends and $K_{\Delta WSA}$ (i.e., trend in ΔWSA; b) across global cities.

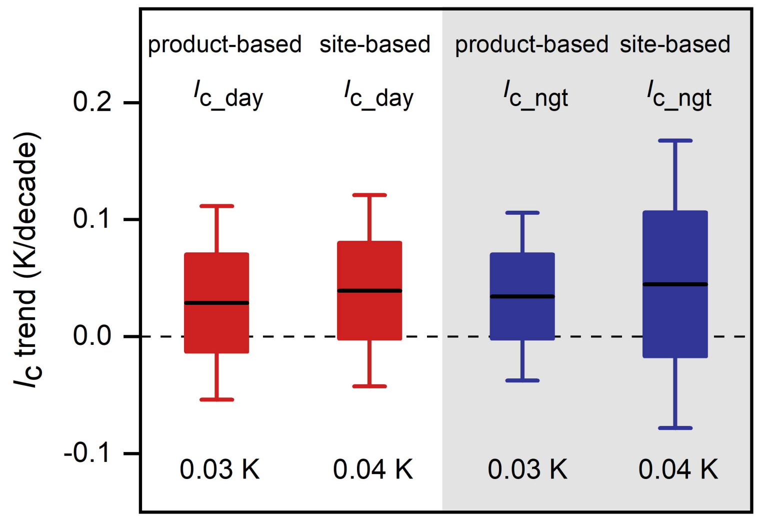

Figure S12. The global mean daytime and nighttime I_c trends quantified based on spatially continuous SAT estimates (termed product-based I_c) and *in-situ* SAT measurements (termed site-based I_c).

Table S1. Details of the data used in this study | The LST, EVI, WSA, LC, AOD, SAT, PREP, RAD are abbreviations for land surface temperature, enhanced vegetation index, white sky albedo, land cover, aerosol optical depth, surface air temperature, precipitation, and radiation, respectively.

Variable	**Product**	**Temporal resolution**	**Spatial resolution**	**Data year**	**References**
LST	MYD11A2	8-day	1 km	2003 to 2020	Ma et al. (2023) Wan et al. (2015)
EVI	MOD13A2	16-day	1 km	2003 to 2020	Didan (2015)
WSA	MCD43A3	16-day	500 m	2003 to 2020	Schaaf & Wang (2015)
LC type	MCD12Q1	Yearly	500 m	2003 to 2020	Friedl & Sulla-Menashe (2019)
AOD	MCD19A2	Daily	1 km	2003 to 2020	Lyapustin & Wang (2018)
SAT	—	Daily	1 km	2003 to 2020	Zhang et al. (2022)
Reanalysis SAT	ERA5-Land	Monthly	0.1 degree	2003 to 2020	Muñoz-Sabater (2019)
Reanalysis PREP	ERA5-Land	Monthly	0.1 degree	2003 to 2020	Muñoz-Sabater (2019)
Reanalysis RAD	ERA5-Land	Monthly	0.1 degree	2003 to 2020	Muñoz-Sabater (2019)
Population	GPWv411	Five years	30 arc sec	2005, 2010, 2015, 2020	Doxsey Whitfield et al. (2015)
Impervious surface area	GAIA	Yearly	30 m	2003 to 2018	Gong et al. (2020)
Global urban boundary	GUB	Five years	—	2000, 2018	Li et al. (2020)

Table S2. The global warming trends based on LST and SAT over both urban and rural surfaces across global 5643 cities.

Trend (°C/decade)	Variable	Urban surfaces	Rural surfaces
day	LST	0.53	0.33
	SAT	0.37	0.34
night	LST	0.53	0.47
	SAT	0.41	0.37
day/night average	LST	0.53	0.40
	SAT	0.39	0.36

Table S3. The abbreviations and symbols used in this study.

Abbreviations	**Descriptions**
UHI	urban heat island
I_s	surface UHI
I_c	canopy UHI
LST	land surface temperature
SAT	surface air temperature
SFP	surface property
BGC	background climate
OUM	overall urban metric
RF	random forest
EVI	enhanced vegetation index
AOD	aerosol optical depth
PREP	precipitation
RAD	shortwave net radiation
ISP	impervious surface percentage
R^2	determination coefficient
ΔAOD	urban-rural contrast in AOD
ΔISP	urban-rural contrast in ISP
ΔEVI	urban-rural contrast in EVI
ΔWSA	urban-rural contrast in WSA
Area	urban area
POP	urban population
K_{POP}	trend in POP
K_{SAT}	trend in SAT
K_{PREP}	trend in PREP
$K_{\Delta\mathrm{AOD}}$	trend in ΔAOD
K_{RAD}	trend in RAD
$K_{\Delta\mathrm{ISP}}$	trend in ΔISP
$K_{\Delta\mathrm{EVI}}$	trend in ΔEVI

$K_{\Delta WSA}$	trend in ΔWSA
ΔDTR_{LST}	urban-rural contrast in LST-based diurnal temperature range
ΔDTR_{SAT}	urban-rural contrast in SAT-based diurnal temperature range
SUCI	surface urban cool island